Calculations of Eddy Current, Fluid, and Thermal Fields in an Air Insulated Bus Duct System

S. L. Ho[1], Y. Li[2], X. Lin[3], Edward W. C. Lo[1], K. W. E. Cheng[1], and K. F. Wong[1]

[1]Department of Electrical Engineering, Hong Kong Polytechnic University, Kowloon, Hong Kong
[2]Research Institute of Special Electrical Machines, Shenyang University of Technology, Shenyang 110034, China
[3]Department of Electrical Engineering, Shenyang University of Technology, Shenyang 110034, China

In this paper, a 3-D eddy-current field model for calculating the eddy current losses in an air insulated bus duct system (AIBDS) is proposed. The temperature rises in the AIBDS, including its long linear section and connecting unit, are evaluated using a coupled fluid field and thermal field model. The contact resistance between the copper conductors and the temperature rise in those contact areas are measured and compared with the simulation results in order to validate the proposed methodology.

Index Terms—Bus duct system (BDS), eddy current loss, temperature rise, thermal fluid.

I. INTRODUCTION

BUS DUCT systems (BDSs) instead of cables are mainly used in low voltage (LV) power distribution systems such as indoor power substations, tall buildings and factories [1]. Most BDS are made of copper conductors with metal enclosures. Recently there are two main types of BDS, the compact BDS (CBDS) and air insulation BDS (AIBDS), which are commonly used in industry. The capacity of CBDS, in which the space between two adjacent copper busbars is only 1–2 mm, is generally larger than other BDS because the enclosure of the former is made of aluminum alloy with excellent heat transfer characteristics. Its eddy-current field covers an open boundary and heat is transferred from the conductors to enclosure mainly by conduction.

AIBDS with a steel enclosure has a close boundary in its eddy current field. Due to the large air space between adjacent conductors and between conductors and enclosure in AIBDS, the copper loss heat energy is transferred, first, from the conductors to the outer enclosure, mainly via convection, and then from the enclosure to the ambient by convection and radiation. Due to the complexity of the heat path, the temperature rise in AIBDS cannot be evaluated readily using traditional heat conduction method only [2], [3]. The coupled eddy current, fluid, and thermal fields must be solved collectively when computing the temperature rise in AIBDS [1]–[3].

The most common design algorithm of AIBDS hitherto is to use lumped circuits together with empirical curves. Recently, the 2-D finite-element model (FEM) are used to analyze the magnetic field distribution of BDS such as AIBDS [3]–[5], CBDS [1], [2], [6], and single- or 3-phase busbars without shielding [7], [8]. A 2-D hybrid FE-boundary element formulation has also been applied in the magnetic field analysis of a four-conductor device with alternating current (ac) supply [7]. In some studies, the electromagnetic (EM) field is computed using FEM with the assumption that the exciting current is
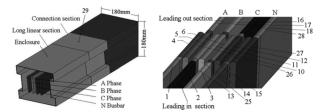

Fig. 1. Schematic structure of an AIBDS showing the basic AIBDS and the location of the measurement points.

equal to the peak value of the steady-state ac current while the eddy current in the conductors is ignored [8]. In all these researches, only the long linear section of the BDS is being modeled and analyzed. Nevertheless, an accurate BDS design requires a 3-D study of the eddy-current field, fluid field, induced magnetic heating, and thermal behaviour of the busbars since the design and analysis include not only the linear section of BDS, but also the different connecting units.

In this paper, 3-D eddy-current field FEM to calculate the losses is described, and then the coupled fluid and thermal fields are solved. The convection of air inside the enclosure and the thermal conduction in the solid materials are also computed. The temperature rises of copper busbars and enclosures in the AIBDS are determined by solving the governing equations. A 1600-A AIBDS, together with its long linear section and connecting unit, is studied and reported. The measured contact resistance and temperature rise in the contact areas between copper conductors are incorporated in the computation.

II. FORMULATION

A. 3-D Eddy-Current Field Model

Fig. 1 shows a typical AIBDS structure. To analyze the losses and thermal problem in the AIBDS, the 3-D eddy-current fields have to be evaluated as described in the following.

Using Maxwell's equation in which the magnetic vector potential and the electric scalar potential are introduced, the eddy-current field equations are written as [9], [10]

$$\left.\begin{array}{l} \nabla \times \nu \nabla \times \dot{\mathbf{A}} - \nabla \nu \nabla \cdot \dot{\mathbf{A}} + \sigma \nabla \dot{\phi} + j\omega\sigma \dot{\mathbf{A}} = 0 \\ \nabla \cdot (-\sigma \nabla \dot{\phi} - j\omega\sigma \dot{\mathbf{A}}) = 0 \end{array}\right\} \text{ in } V_1 \quad (1)$$

$$\nabla \times \nu \nabla \times \dot{\mathbf{A}} - \nabla \nu \nabla \cdot \dot{\mathbf{A}} = \dot{\mathbf{J}}_s \quad \text{in } V_2 \tag{2}$$

where V_2 is the source current area, V_1 is the other area without source current, and V is the whole solved area.

The boundary conditions are

$$\left. \begin{array}{l} \mathbf{n} \times \dot{\mathbf{A}} = 0 \\ \nu \nabla \cdot \dot{\mathbf{A}} = 0 \end{array} \right\} \quad \text{in } S_1 \tag{3}$$

$$\left. \begin{array}{l} \nu \nabla \times \dot{\mathbf{A}} \times \mathbf{n} = 0 \\ \mathbf{n} \cdot \dot{\mathbf{A}} = 0 \end{array} \right\} \quad \text{in } S_2 \tag{4}$$

$$\left. \begin{array}{l} \dot{\mathbf{A}}_1 = \dot{\mathbf{A}}_2 \\ \nu_1 \nabla \cdot \dot{\mathbf{A}}_1 = \nu_2 \nabla \cdot \dot{\mathbf{A}}_2 \\ \nu_1 \nabla \times \dot{\mathbf{A}}_1 \times \mathbf{n}_{12} = \nu_2 \nabla \times \dot{\mathbf{A}}_2 \times \mathbf{n}_{12} \\ \mathbf{n} \cdot (-j\omega\sigma\dot{\mathbf{A}} - \sigma\nabla\dot{\phi}) = 0 \end{array} \right\} \quad \text{in } S_{12}. \tag{5}$$

Introducing the boundary condition, the weighted residue equation can be written as

$$\int_V (\nu \nabla \times \mathbf{N}_i \cdot \nabla \times \dot{\mathbf{A}} + \nu \nabla \cdot \mathbf{N}_i \nabla \cdot \dot{\mathbf{A}} + j\omega\sigma\mathbf{N}_i \cdot \dot{\mathbf{A}}$$
$$+ \sigma\mathbf{N}_i \cdot \nabla\dot{\phi} - \mathbf{N}_i \cdot \dot{\mathbf{J}}_s)dv = 0 \quad \text{in } V \tag{6}$$

$$\int_{V_1} \nabla N_i \cdot (j\omega\sigma\dot{\mathbf{A}} + \sigma\nabla\dot{\phi})dv = 0 \quad \text{in } V_1 \tag{7}$$

where N_i is the weighted function. In the model, the uniqueness condition can be satisfied. The boundary condition and the source current are readily included in the evaluation of the magnetic flux, eddy-current profiles, and heat loss.

B. Thermal Equations

At steady state, the thermal problem of the CBDS satisfies the following thermal equilibrium equation:

$$P_K + P_M = Q_{KD} + Q_{KF} \tag{8}$$

where P_M and P_K are the power losses in Joule, respectively, in the phase busbars and the enclosure, Q_{KD} and Q_{KF} are, respectively, the heat loss from the enclosure to the surrounding air by radiation and convection.

In AIBDS, the radiation heat is negligibly small and heat loss is transferred mainly by natural convection from the conductors to the enclosure and from the enclosure to the surrounding air. The natural convection inside the AIBDS satisfies the following Navier–Stokes equations [1]:

$$\frac{\partial(\rho u)}{\partial x} + \frac{\partial(\rho v)}{\partial y} + \frac{\partial(\rho w)}{\partial z} = 0 \tag{9}$$

$$\rho u \frac{\partial u}{\partial x} + \rho v \frac{\partial u}{\partial y} + \rho w \frac{\partial u}{\partial z} = \mu \nabla^2 u - \frac{\partial P}{\partial x} + Sx \tag{10}$$

$$\rho u \frac{\partial v}{\partial x} + \rho v \frac{\partial v}{\partial y} + \rho w \frac{\partial v}{\partial z} = \mu \nabla^2 v - \frac{\partial P}{\partial y} + Sy \tag{11}$$

$$\rho u \frac{\partial w}{\partial x} + \rho v \frac{\partial w}{\partial y} + \rho w \frac{\partial w}{\partial z} = \mu \nabla^2 w - \frac{\partial P}{\partial z} + Sz \tag{12}$$

$$\rho c u \frac{\partial T}{\partial x} + \rho c v \frac{\partial T}{\partial y} + \rho c w \frac{\partial T}{\partial z} = k \nabla^2 T + Q \tag{13}$$

where ρ is fluid density, μ is viscosity coefficient, c is the specific heat, k is the coefficent of heat conductivity, u, v, w are the respective x-, y-, z-direction potentials of the fluid speed, P is the fluid pressure, T is the fluid temperature, S_x, S_y, and S_z are the sources in the respective x-, y-, and z-directions, and Q is the heat value per unit volume.

In the computation, the ambient temperature is set to 40 °C. The heat sources in AIBDS are the losses in the busbars and enclosures. The heat transfer coefficient is an empirical parameter that takes care of the heat transfer relationship and the nature of air flow patterns near the surfaces, the air properties as well as the geometry of the outside surfaces as determined by the nondimensional parameters that include the Grashof (Gr), Prandtl (Pr), Rayleigh (Ra), and Nusselt (Nu) numbers [1], [3].

The Nusselt number can be represented by a power law

$$\text{Nu} = C(\text{Gr} \cdot \text{Pr})^n. \tag{14}$$

The Grashof number is defined by the following:

$$\text{Gr} = \left(\frac{g\beta\Delta T L^3}{v^2} \right). \tag{15}$$

where g is the gravitational acceleration, β is the coefficient of thermal expansion, θ is the temperature difference, L is the equivalent linear dimension, and ν is the kinematic viscosity.

The Prandtl number is given by

$$\text{Pr} = \frac{\nu}{\alpha} \tag{16}$$

where α is the thermal conductivity of the fluid (air in this case) and C and n are dimensionless constants dependent on the system. For the case being studied, n equals to 0.25, C equals to 0.59 for the vertical surfaces, 0.27 for the upper horizontal surface, and 0.54 for the lower horizontal surface [3].

The Nusselt number is a nondimensional heat transmission coefficient defined by the following equation (applicable at steady state) [1]:

$$\text{Nu} = \frac{h_c L}{\alpha\theta} \tag{17}$$

where h_c gives a measure of the heat quantity transferred per unit time and per unit area to the outside busbar surfaces. For the system being studied, the coefficient h_c (W/m^2 K) is 5.436 for the vertical surfaces, 3.082 for the upper horizontal surface, and 6.164 for the bottom surface.

III. CALCULATIONS AND TEST OF A 1600-A AIBDS

A 1600-A AIBDS structure has been designed and built. Its eddy-current field, losses, fluid, and temperature rises are computed using the proposed algorithm. In the computation of the eddy-current field, the rated source current is 1.6 kA and the 3-phase source currents are assumed to be $(-1.1312 + j1.959)$ kA in phase A, $(2.2624 + j0)$ kA in phase B, and $(-1.1312 - j1.959)$ kA in phase C. The total elements and nodes are 33777 and 19012 and there are 61774 unknown variables. The computation time is 153 min using a Pentium-IV Computer (2.6 GHz and 1-G memory). The source programs (FE method) such as mesh generation, stiffness matrix generation, and the equation solver are written in Fortran. The relative permeabilities of the copper conductor and steel enclosure are assumed to be 1 and 500, respectively. Tables I and II also give, respectively, the main geometrical and material properties of the analyzed model.

TABLE I
MAIN GEOMETRY DATA OF THE ANALYZED MODEL

Width of conductor (mm)	Height of conductor (mm)	Separation of adj. conductors (mm)	Width of enclosure (mm)	Height of enclosure (mm)	Thickness of enclosure (mm)
8	130	12	180	180	1.5

TABLE II
MATERIAL DATA OF THE ANALYZED MODEL

Material	Thermal conductivity (W/K/m)	Specific heat (J/ kg/K)	Density (kg /m^3)	Resistivity ($10^{-8}\Omega\cdot$m)
Copper conductor	399	385	8933	1.65×(1+ 0.004×T)
Steel enclosure	43.2	460	7850	9.7
Insulation	0.043	1.026	34.8	-

where T is temperature of the copper conductor (°C)

TABLE III
LOSSES IN THE BUSBARS AND ENCLOSURE IN A 1600 A AIBDS (W/M)

N-phase busbar	A-phase busbar	B-phase busbar	C-phase busbar	Enclosure
0.46	94.2	98.4	93.7	4.6

Table III gives the losses of the busbars and enclosure in the scheme.

It is found from simulation that there are eddy currents in both the N-phase busbar and enclosure. The total losses of the AIBDS is 291.4 W/m. That includes 286.3 W/m in the A-, B-, and C-phase busbars and 5.06 W/m in the enclosure and N-phase busbar. As the resistivity of the copper busbars and the convective heat transfer coefficient are temperature dependent, their effects must be included in the eddy-current field and thermal equations. The governing equation, thus, derived is then solved iteratively by assuming, first, an initial temperature rise in the copper conductors and enclosures. If the error between the calculated temperature and the initial temperature assumed is larger than ε (ε is assumed to be 10%), the initial temperature needs to be modified and then the convective heat transfer coefficient of the enclosure, the resistances, losses, and temperatures of the copper conductors and the enclosure are calculated all over again.

Fig. 2 shows the EM field pattern on a cross section of the AIBDS and Fig. 3 illustrates the distribution of the temperature, which has the maximum on the B-phase conductor. As the air is being heated, it flows upwards along the space between the adjacent phase conductors and then downwards along the space between the copper conductor and side plate of the enclosure and then circulates as shown in Fig. 4. The fluid speed can reach 0.19 m/s. Because of this, the maximum temperature in the enclosure are observed on its upper surface as shown in Fig. 5, and it is higher than the corresponding one on the down surface by about 8 K.

In order to check whether the AIBDS complies with the design, an experimental bus duct is built and tested. In the test, the temperature of a horizontal busbar with vertical copper conductors located at a distance of 200 mm from the ground is measured. The conductors are fed from one side with a low voltage 3-phase supply. The other sides of the busbars are short
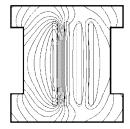

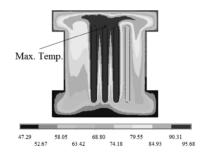Fig. 2. Electromagnetic field on a cross section of the AIBDS.

47.29	58.05	68.80	79.55	90.31
52.67	63.42	74.18	84.93	95.68

Fig. 3. Temperature in the AIBDS.

| 0.0 | 0.021 | 0.042 | 0.064 | 0.085 | 0.106 | 0.128 | 0.149 | 0.170 | 0.192 |

Fig. 4. Fluid field in the AIBDS.

Hottest spot

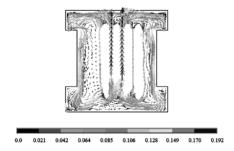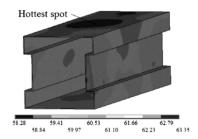| 58.28	59.41	60.53	61.66	62.79
58.84	59.97	61.10	62.23	63.35

Fig. 5. Enclosure temperature profile.

circuited. The neutral phase is not connected. The temperature measurements are taken using thermocouples. The results of the test indicate that the temperature rise in the measured points on the busbar is in good agreement with the computed result. Table IV gives the test and computed temperature rise results (measurement positions are as shown in Fig. 1). It can be seen that the hottest spot in the busbar and in enclosure are lower than the respective maximum temperature rise limits of 30 and 70 K of the AIBDS. Close agreement between the computed and measured temperature rise on the busbars, as shown in Table IV, can be seen as a good validation of the proposed methodology.

Fig. 6 shows the temperature rise in the AIBDS, with curves 1, 2, and 3 corresponding to the temperature rises in the B-phase busbar, the N-busbar, and the enclosure, respectively.

Sections of busbars in AIBDS are usually bolted together electrically. The contact resistance of the connecting parts is one of the main factors influencing the thermal performance of

TABLE IV
TESTED AND CALCULATED RESULTS OF TEMPERATURE RISE (K)

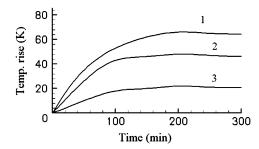| Measured point	Tested	Computed	Error (%)
1	61.3	57.72	5.3
2	63.8	62.65	1.8
3	60.6	57.65	7.3
4	61.7	58.21	8.4
5	64.4	63.49	0.4
6	61.5	58.01	6.2
10	63.8	58.21	9.7
11	65.9	63.50	4.0
12	62.3	58.10	8.1
16	61.6	57.32	8.8
17	63.4	62.23	1.7
18	61.3	57.02	8.0
25	43.0	39.15	4.9
26	46.4	43.52	7.3
27	46.4	43.53	4.6
28	43.6	40.02	4.1
29 (Enclosure)	20.8	22.79	7.9

Fig. 6. Time variation of temperature rises during the test.

TABLE V
MEASURED CONTACT RESISTANCE OF TWO CONDUCTORS ($\mu\Omega$)

	1	2	3	4	5	6	7	8	Average
A phase	1.7	2.2	1.4	2.1	2.3	0.9	1.8	2.7	1.89
B phase	2.2	1.6	1.8	2.3	3.0	2.1	2.3	1.9	2.15
C phase	2.8	2.6	2.0	2.8	2.3	1.8	1.9	2.7	2.24

AIBDS, because the contact resistance could have significant bearings upon the temperature rises in the busbars. Indeed, the temperature rise at the contact is generally higher than those in the other sections such as in the long linear sections of most AIBDS. Obviously, the contact resistance is governed by factors such as the material characteristics, contact condition, contact pressing force and the degree of oxidization or state of sulfuration at the contact surfaces of the copper conductors. Thus, a pure computation of the contact resistance is difficult and the contact resistance between two sections of the busbars as well as the temperature rises at the connecting sections of the AIBDS are measured. Table V shows the contact resistances, which is the average of eight measurements, in the 3-phase copper conductors. As mentioned earlier, Table IV gives the temperature rise in the connecting sections of the AIBDS. It can be seen that the differences in temperature rise at the measuring positions in the same phase are small.

The influence of the gap space between the two adjacent phases upon the temperature rise of busbars have also been
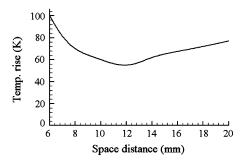

Fig. 7. Variation of temperature rise in the B-phase conductor against the space distance between two adjacent phase conductors.

investigated. In this study, the space distance is changed from 6 to 20 mm, whereas the current ratings and busbar sizes are assumed constant. The corresponding temperature rise of the copper conductors in the B-phase are shown in Fig. 7. It can be seen that the busbar temperature decreases as the gap between the two adjacent phase conductors increases until it reaches a minimum at 12 mm. Upon careful consideration of the thermal and fluid factors, the distance of the adjacent phase conductors is chosen as 12 mm in the final design.

IV. CONCLUSION

Unlike other research results presented before, a 3-D eddy-current field method is described for the computation of eddy current losses in an AIBDS in this paper. By solving the thermal equations, fluid equations, and eddy-current field, the temperature rises of the busbars, the enclosure, the long linear section, and the connecting section in the AIBDS are all determined and analyzed. The calculated and test results are found to be in good agreement.

REFERENCES

[1] A. B. Wu, "Finite element analysis of coupled magneto-thermal fields for compact busbar tranking system," *High Voltage Appar.*, vol. 39, no. 4, pp. 7–10, 2003.
[2] C. C. Hwang, "Analysis of electromagnetic and termal fields for a bus duct system," *Electr. Power Syst. Res.*, vol. 45, no. 1, pp. 39–45, 1998.
[3] H. Hedia, "Arrangement of phases and heating constraints in a busbar," *IEEE Trans. Magn.*, vol. 35, no. 3, pp. 1274–1277, May 1999.
[4] R. T. Coneybeer, "Steady state and transient ampacity of busbar," *IEEE Trans. Power Delivery*, vol. 9, no. 4, pp. 1822–1829, 1994.
[5] S. W. Kim, "Coupled finite element analytic technique for prediction of temperature rise in power apparatus," *IEEE Trans. Magn.*, vol. 38, no. 2, pp. 921–924, Mar. 2002.
[6] Y. Du, J. Burnett, and Z. C. Fu, "Experimental and numerical evaluation of busbar trunking impedance," *Electr. Power Syst. Res.*, vol. 55, no. 2, pp. 113–119, Aug. 2000.
[7] O. Bottauscio and E. Carpaneto, "Numerical and experimental evaluation of magnetic field generated by power busbar systems," *IEE Proc. Gener. Trans. Distrib.*, vol. 143, no. 5, pp. 455–460, Sep. 1996.
[8] D. G. Triantafyllidis, "Parametric short circuit force analysis of three phase busbar—A fully automated finite eelment approach," *IEEE Trans. Power Delivery*, vol. 18, no. 2, pp. 531–536, Apr. 2003.
[9] O. Biro and K. Preis, "On the use of the magnetic vector potential in the finite element analysis of three dimensional eddy currents," *IEEE Trans. Magn.*, vol. 25, no. 4, pp. 3145–3159, Jul. 1989.
[10] D. X. Xie, "Vector potential and electrical scalar potential in 3D eddy current calculations," *Proc. Electromagn. Field Electr. Eng. BISEF*, pp. 312–316, 1988.